

Femtosecond pulse pair distribution functions at MID at the European XFEL

Robert P.C. Bauer^{1,2*}, Alexander Gierke^{1,3}, Claudia Goy¹, Jan-Etienne Pudell³, Wonhyuk Jo³, Joana Valerio³, Luigi Adriano³, Johannes Möller³, James Wrigley³, Ulrike Boesenberg³, Angel Rodriguez-Fernandez³, Roman Shayduk³, Mohamed Youssef³, Nele N. Striker¹, Niels C. Giesselmann¹, Svenja C. Hövelmann^{1,4}, Wojciech Roseker¹, Kartik Ayyer^{5,6}, Michael Paulus⁷, Christian Sternemann⁷, Robert E. Grisenti^{8,9}, Anders Madsen³, Joachim Schulz³, and Felix Lehmkuhler^{1,6}

¹ Deutsches Elektronen-Synchrotron DESY, Hamburg, Germany

² Freiberg Center for Water Research, TU Bergakademie Freiberg, Freiberg, Germany

³ European X-ray Free Electron Laser Facility, Schenefeld, Germany

⁴ Institute of Experimental and Applied Physics, Kiel University, Kiel, Germany

⁵ Max Planck Institute for the Structure and Dynamics of Matter, Hamburg, Germany

⁶ The Hamburg Centre for Ultrafast Imaging, Hamburg, Germany

⁷ Fakultät Physik/DELTA, Technische Universität Dortmund, Dortmund, Germany

⁸ Institut für Kernphysik, J. W. Goethe-Universität Frankfurt(M), Frankfurt(M), Germany

⁹ GSI Helmholtzzentrum für Schwerionenforschung GmbH, Darmstadt, Germany

*E-mail: robert.bauer@desy.de

Abstract. Pair distribution functions from individual femtosecond X-ray pulses have the potential to elucidate the structure of transient states in matter, such as those found in liquid systems. To demonstrate this possibility an experiment was conducted at the Materials Imaging and Dynamics instrument of European X-ray Free Electron Laser Facility. We utilized the large field of view detector configuration, exploiting single high-flux X-ray pulses of femtosecond duration at 23 keV photon energy. After deconvolution from the pattern termination function, we show here pair distribution functions of liquid water at approximately 260 K. These results demonstrate that current X-ray free electron laser methods can acquire pair distribution functions on the femtosecond timescale that have potential to capture transient state of liquids.

1. Introduction

The pair distribution function (PDF) method, developed in 1930 by Debye and Menke [1], is a useful tool to retrieve real space atomic distances from scattering experiments. PDFs describe the interatomic distance in a material. Specifically, for scattering experiments the atomic structure factor of the scattering sample is transformed through a sine Fourier transform to retrieve the pair spacing [2-4]. Recent developments in X-ray free electron lasers (XFEL), provide the potential to measure PDFs in femtosecond snapshots of systems that used to be averaged over hour long acquisitions [5-10]. Probing the transient properties of bulk structures is challenging within standard X-ray studies as the nature of the sample is typically averaged during a measurement,



Content from this work may be used under the terms of the [Creative Commons Attribution 4.0 licence](https://creativecommons.org/licenses/by/4.0/). Any further distribution of this work must maintain attribution to the author(s) and the title of the work, journal citation and DOI.

due to the large sampled volume and long-time scale of the measurement. The rapid acquisition time of XFELs offers a way to obtain PDFs, facilitating the understanding of the structure of transient states in matter. The high photon density of XFEL radiation poses additional considerations in terms of sample environment. Specifically, to avoid probing beam induced effects, the sample must be refreshed for every pulse to exploit the full potential of this method. Hence, liquids are ideal samples for such experiments. Liquid jet sample environments have become a standard for rapid sample delivery, that enable one to measure samples free of container background while maintaining small sample volumes [11].

This investigation strives to provide a method to conduct PDF analysis at the Materials Imaging and Dynamics (MID) instrument of European XFEL using femtosecond X-ray pulses. We focus on X-ray diffraction in a “large field of view” (LFOV) configuration to enable the use of PDF analysis [12], which require a large range of momentum transfer (q -range) to be covered. We demonstrate the capability of collecting single-pulse scattering patterns suitable for PDF analysis if proper detector calibrations are applied.

2. Method

The experiment was conducted at MID [12, 13], using the multipurpose chamber with the liquid jet system mounted on a hexapod. The liquid jet utilized a glass Rayleigh nozzle with an exit orifice of 11 μm diameter [11]. For demonstration purposes a sample of ultrapure Millipore water (18.2 $\text{M}\Omega\cdot\text{cm}$) was measured. Additional shielding and differential pumping apparatus were installed to improve the chamber vacuum to reach 10^{-5} mbar pressure. This specific vacuum requirement is due to the high voltage components of the Adaptive Gain Integrating Pixel Detector (AGIPD) that is connected directly to the sample chamber. Additional Kapton foils were used for separation of the AGIPD and sample chamber serving to further improve the detector vacuum and mitigate pressure spikes inherent in liquid jet experiments. The sample interaction point was positioned at $z = 17.7$ cm upstream the detector, with the European XFEL supplying 23 keV photons in femtosecond pulses (< 50 fs) at pulse energies of 120 μJ and a repetition rate of 2.2 MHz in 10 Hz bursts. The beam was focused to a spot size of ~ 5 μm (FWHM) at the interaction point using compound refractive lenses.

2.1 Detector calibration

AGIPD at MID works in a 1M configuration with the ability to move the four detector quadrants independently depending on the experiment requirements [14, 15]. Typical experiments so far have primarily used the detector in a small angle configuration with sample-detector distances of ~ 8 m. Recently Möller et al. have reported the results of an experiment using the LFOV configuration at MID studying nucleation in liquid cryo-jets at 9 keV [16]. Here, we report the first experiment at MID using a high photon energy of 23 keV, together with the short sample to detector distance. This allows the capture of scattering momentum transfer up to ~ 9 \AA^{-1} on the detector. Thus, refinements of the detector quadrant positions are required for precise measurements. Figure 1a) shows a photograph of the AGIPD before it is mounted to the vacuum chamber. When tracing the mirrored images of the MID hutch on the individual detector modules one can see that the detector module surfaces are not perfectly aligned in a plane relative to each other. Figure 1b) depicts the detector geometry assuming a fixed distance between the sample and detector planes, i.e. no tilts or rotations of the detector quadrants. The PyFAI graphic user interface [17] was used to calibrate the modules using a LaB_6 reference sample. The LaB_6 reference measurements were averaged over the sample movement perpendicular to the beam to

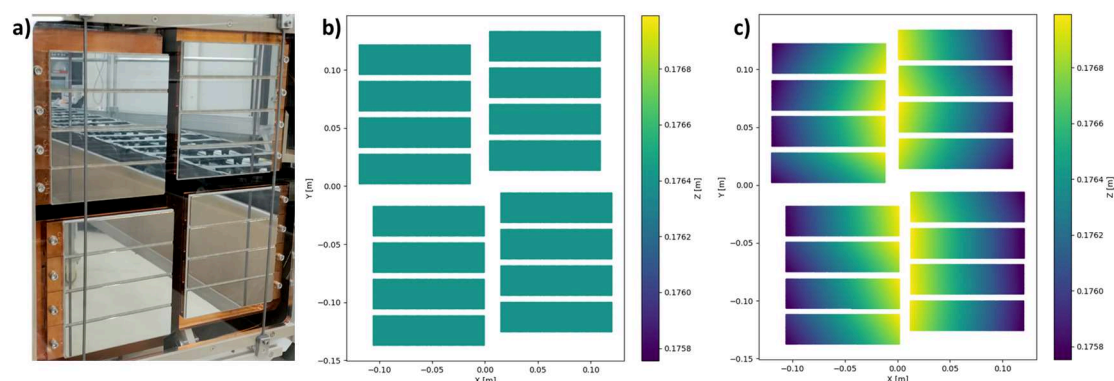


Figure 1. AGIPD 1M Calibration a) photograph of detector modules, b) initial assumption with single plane of detector quadrants, c) final calibration of individual modules, indicating inwards tilting by ~ 10 mrad. Parts b) and c) use cartesian coordinates centered at the sample, with the z-axis parallel to the beam direction, with the x-axis horizontal and y-axis vertical perpendicular to the beam.

capture full powder diffraction rings. The individual module calibration was possible due to the large number of Bragg reflections observed from edge to edge of the modules in this configuration. Subsequent integration utilized the PyFAI multi-geometry algorithm to normalize the solid angle contribution from detected photons. Figure 1c visualizes the corrected geometry for the detector considering each of the 16 modules independently. An azimuthal integration of a measured LaB6 reference is shown in Figure 2a) highlighting the impact of including the previously described tilt of each detector module for the resulting q -calibration. Compared to the planar assumption q -values are shifted up 0.046 \AA^{-1} for low q -values and down 0.010 \AA^{-1} at high q -values in our measurement geometry. The full width half maximum reduced by approximately half due to the refinement of detector calibration, for the 1.512 \AA^{-1} feature it changed from $\sim 0.044 \text{ \AA}^{-1}$ to $\sim 0.024 \text{ \AA}^{-1}$. Several approaches were attempted when calibrating the detector surface, including calibrating the separate quadrants of the detector. However, variability on the module level necessitated the individual module method.

3. Results and Discussion

Figure 2 (b-c) illustrate the PDF analysis of single pulse scattering from water at a distance of 3.9 mm from the nozzle yielding an estimated temperature of ~ 260 K. The part b) of Figure 2 shows a scattering pattern collected from a single XFEL pulse at 23 keV. Integrating the azimuthal component of the sample pattern of Figure 2b) and considering the q -calibration of Figure 2a), we obtain the $I(q)$ distribution depicted in part c) of Figure 2. The outermost fringes of the diffraction pattern are captured by a reduced number of pixels due to the geometry of the detector decreasing the signal to noise ratio. This increase in noise at large q , necessitates further truncation than that of the physical area of the detector modules. Figure 2d) shows the corresponding PDF of the Figure 2c). The blue PDF G_c , was computed using the pdfgetx3 software

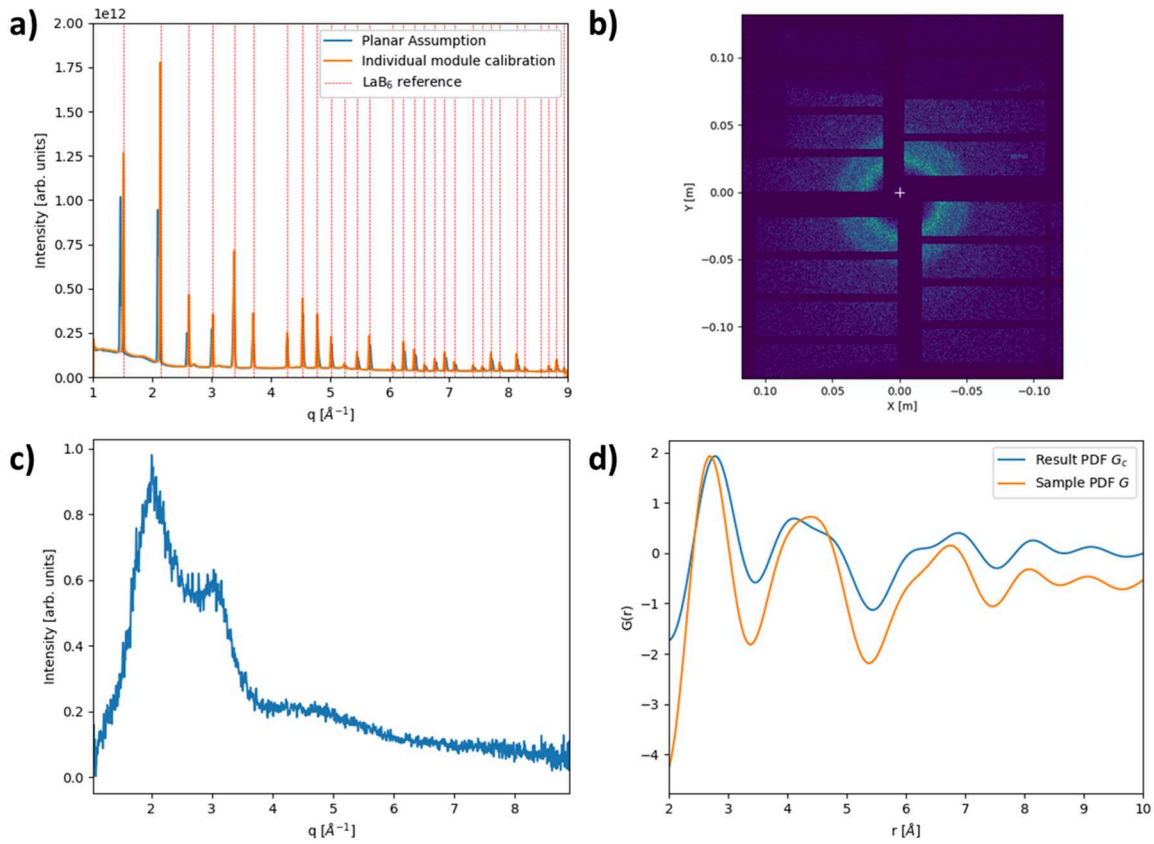


Figure 2. a) Comparison between (blue) initial detector geometry assumption and (orange) individual module calibration of LaB₆ calibrant with (dashed red) reference LaB₆ reflections. Femtosecond single pulse scattering from water and respective analysis in parts b), c) and d); b) raw detector image; c) 1D integration; d) resulting PDF G_c from 1D integration, blue, and sample PDF G resulting from the deconvolution with termination function, orange, rescaled for comparison.

written and maintained by Billinge's group [18] and is referred to as PDF G_c . Due to the truncation of the q -range to between 1.08 \AA^{-1} and 6.38 \AA^{-1} there is a significant contribution from the termination function.

The termination function

$$\theta(r, q_{min}, q_{max}) = \begin{cases} 1 & \text{if } q_{min} \leq q \leq q_{max} \\ 0 & \text{otherwise} \end{cases} \quad (1)$$

is one in the region of the pattern where there is signal and zero otherwise, where q_{min} and q_{max} are the respective termination values of the momentum transfer q -range covered by AGIPD. Consider the formulation by Peterson et al. [19] of the Fourier transform of the termination function

$$\theta(r, q_{min}, q_{max}) = \frac{q_{max}}{\pi} j_0(q_{max}r) - \frac{q_{min}}{\pi} j_0(q_{min}r) \quad (2)$$

where the zeroth order Bessel function is denoted by j_0 . Figure 3 depicts the impact of termination: a) no termination, b) truncation of the q_{max} , and c) truncation of both q_{min} and q_{max} .

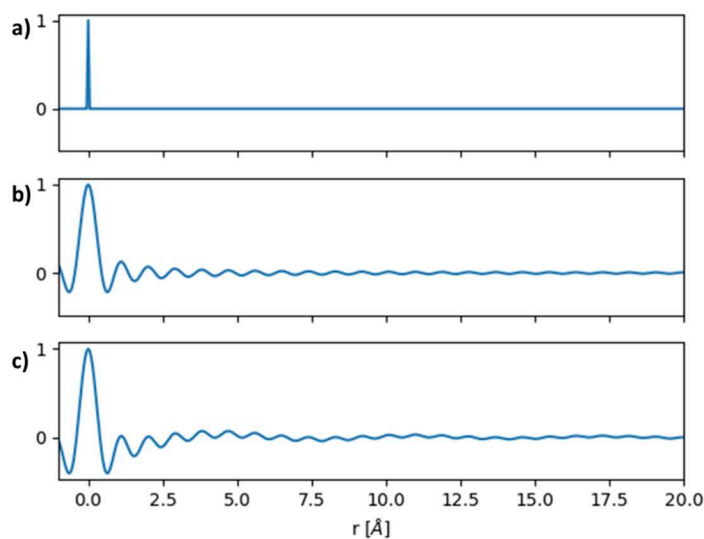


Figure 3. Fourier transform of termination function demonstrating the response function to be convolved with the sample pair distribution function, normalized for comparison; a) no termination b) terminated at $q_{\max} = 7 \text{ \AA}^{-1}$ c) terminated at $q_{\min} = 1 \text{ \AA}^{-1}$, $q_{\max} = 7 \text{ \AA}^{-1}$

Note that in the absence of termination the function is essentially a delta function. Truncation of the maximum q introduces high frequency fringes; a truncation of minimum q adds a low frequency component.

Following this concept, the resulting convoluted PDF (G_c) from the $I(q)$ data can be seen as the convolution of the true sample PDF (G) with θ the Fourier transform of the termination function which depends on the experiment geometry as

$$G_c(r) = G(r) * \theta(r, q_{\min}, q_{\max}) \quad (3)$$

Thus, by performing the deconvolution of the G_c PDF with the Fourier transformed termination function we retrieve G , the samples PDF which is depicted in Figure 2d) by the orange PDF. One can see a shift of the first peak position to lower r for G and a variation in the shape of the second feature. The G PDF shown in figure 2d) does not oscillate about zero as G_c , this is being investigated as a need to correct for an incorrect high- q asymptote [19]. There are other treatments of the termination function and truncation errors in literature such as that of Skinner et al. [20] where they use a modified Lorch function building upon the work of Soper and Barney [21]. Naberukhin [22] comments on the results of Skinner et al. noting that further consideration is needed, specifically likening the approach to that of Narten et al. [23]. The modified Lorch function of Skinner et al. is specifically adapted to water to smoothing impact on the first peak. Here we focus only on the experimental constraints when addressing the termination function in a general way independent of the sample.

5. Conclusion

We show the feasibility PDF analysis on femtosecond diffraction patterns of a liquid sample. We found that for the small sample to detector distance in the LFOV configuration at MID the pixel geometry of AGIPD 1M requires further calibration, specifically considering the tilt of each

quadrant and individual modules. Refinement of the detector calibration eliminated artefacts which interfered with PDF analysis. The termination function is inherent in scattering experiments with a limited q -range, and must be considered when comparing results from different experiments. Thanks to understanding the termination function, direct comparison of PDFs covering a q -region with ones that sample larger regions is possible. However, increasing the sampled q -region is the best method to improve the quality of the results. Standard methods of increased photon energy or increased sampling area, are required with additional consideration of the individual detector design. Further progress is planned for XFEL facilities which would see higher photon energy and density, enabling higher q sampling with comparable detector areas and increased scattering signal. There is a need for high- Z detector to facilitate higher photon energies that would further extend the measurable momentum transfer region.

Acknowledgments

We acknowledge European XFEL in Schenefeld, Germany, for provision of X-ray free-electron laser beamtime at Scientific Instrument MID (Materials Imaging and Dynamics) under proposal number P003422 and would like to thank the staff for their assistance. This work was carried out in the framework of the 2022 EuXFEL Call on Molecular Water Science. We also acknowledge the scientific exchange and support of the Centre for Molecular Water Science (CMWS). This research was supported by the CMWS in an Early Science Project. We also acknowledge the scientific exchange and support of the Zentrum für Wasserforschung Freiberg (ZeWaF). This research was supported in part through the Maxwell computational resources operated at Deutsches Elektronen-Synchrotron DESY, Hamburg, Germany. This work is supported by the Cluster of Excellence 'Advanced Imaging of Matter' of the Deutsche Forschungsgemeinschaft (DFG) - EXC 2056 - project ID 390715994.

References

- [1] P. Debye, and H. Menke, 1930. *Phys. Z.*, 31, 797-798.
- [2] H.P. Klug, and L.E. Alexander, 1974. *John Wiley and Sons*, New York, 791-859.
- [3] T. Egami, and S.J. Billinge, 2012. *Pergamon*, 2nd edition, Vol. 16.
- [4] S.J. Billinge, 2019. *Philosophical Transactions of the Royal Society A*, 377(2147), 20180413.
- [5] B.E. Warren, H. Krutter, and O. Morningstar, 1936. *J. Am. Ceram. Soc.*, 19(1-12), 202-206.
- [6] G.S. Cargill III, 1975. *Solid State Physics*, 30, 227-320.
- [7] C.N.J. Wagner, 1978. *Journal of Non-Crystalline Solids*, 31(1-2), 1-40.
- [8] D.D. Kofalt, et al., 1986. *Physical review letters*, 57(1), 114.
- [9] T. Egami, and S.J. Poon, 1988. *Materials Science and Engineering*, 99(1-2), 323-329.
- [10] A.H. Narten, W.E. Thiessen, and L. Blum, 1982. *Science*, 217(4564), 1033-1034.
- [11] A. Gierke, et al., 2024. *J. Phys.: Conf. Ser.*, SRI 2024, (submitted).
- [12] A. Madsen, et al., 2021. *J Synchrotron Radiat.*, 28, 637-649.
- [13] R. Bauer, F. Lehmkuhler et al., 2023. p003422, <https://doi.org/10.22003/XFEL.EU-DATA-003422-00>.
- [14] A. Allahgholi, et al., 2019. *Nucl. Instrum. Meth. A* 942, 162324.
- [15] J. Sztuk-Dambietz, et al., 2023. *Frontiers in Physics* 11, 1329378.
- [16] J. Möller, et al., 2024. *Physical review letters*, 132(20), 206102.
- [17] J. Kieffer, et al., 2020. *Journal of synchrotron radiation*, 27(2), 558-566.
- [18] P. Juhás, et al., 2013. *Journal of applied crystallography*, 46(2), 560-566.
- [19] P.F. Peterson, et al., 2003. *Journal of applied crystallography*, 36(1), 53-64.
- [20] L. B. Skinner, et al., 2013. *The Journal of Chemical Physics*, 138(7).
- [21] A.K. Soper, and E.R. Barney 2012. *Journal of Applied Crystallography*, 45(6), 1314-1317.
- [22] Y.I. Naberukhin, 2017. *Journal of Molecular Liquids*, 239, 45-48.
- [23] A.H. Narten, C.G. Venkatesh, and S.A. Rice, 1976. *The Journal of Chemical Physics*, 64(3), 1106-1121.